High-Intensity Fast-Response Electric radiant Panel (HIFREP) to impose fire equivalent heat fluxes on building elements with enhanced thermal boundary conditions accuracy

Florian Put[1]*, Balša Jovanović[2], Evelien Symoens[3], Andrea Lucherini[4], Bart Merci[5], Ruben Van Coile[6]

[1] PhD student, Department of Structural Engineering and Building Materials, Ghent University, Belgium. ORCID: 0000-0002-4522-9015

[2] PhD student, Department of Structural Engineering and Building Materials, Ghent University, Belgium. ORCID: 0000-0001-5200-5848

[3] PhD student, Department of Structural Engineering and Building Materials, Ghent University, Belgium. ORCID: 0000-0002-0414-3258

[4] PhD, Senior Researcher, Department for Research of Fire-Safe Sustainable Environment (FRISSBE), Slovenian National Building and Civil Engineering Institute (ZAG), Slovenia. ORCID: 0000-0001-8738-1018

[5] Professor, Department of Structural Engineering and Building Materials, Ghent University, Belgium. ORCID: 0000-0002-2600-0098

[6] Professor, Department of Structural Engineering and Building Materials, Ghent University, Belgium. ORCID: 0000-0002-9715-6786

* Corresponding author. E-mail: Florian.Put@UGent.be.

ABSTRACT

Bench-scale fire testing has gained popularity as a highly controllable and cost-effective solution, overcoming many of the shortcomings of traditional large-scale fire resistance tests. Whereas gas-fired radiant panels have demonstrated significant success in this area, the present study introduces a novel High-Intensity Fast-Response Electric radiant Panel (HIFREP). Utilizing electrically operated radiation emitters, it provides more precise and quasi-instantaneous control over the thermal boundary conditions. HIFREP delivers high and stable heat fluxes up to 105 kW/m², and, due to the low thermal inertia of the emitters, can rapidly adjust its output to changes in the input. In this regard, the time constant of the emitters has been found to be less than 1 s, both during heating and cooling. It eliminates gas combustion and hence avoids the need for extraction hoods when testing the fire performance of non-combustible materials, making it suitable for traditional structural testing laboratories. The presented High-Intensity Fast-Response Electric radiant Panel also provides a reliable tool for the validation of FEM simulation results by accurately replicating the thermal boundary conditions in structural fire engineering analyses.

KEYWORDS

Radiant panel, Fire testing, Heat transfer, Radiation, Heat flux, Thermal boundary conditions

1 INTRODUCTION

Many building products, elements and systems require detailed assessment of their behaviour when exposed to fire conditions (i.e., elevated temperatures and high heat fluxes). From a structural perspective, fire testing typically includes the investigation and assessment of mechanical behaviour at elevated temperatures, as well as structural capacity and integrity when exposed to fire conditions [1]. Furthermore, sustainability targets are changing the built environment, and fire safety evaluations are becoming more and more relevant in the construction industry [2].

As regards the assessment of the performance of building elements exposed to post-flashover fires, the current framework involves standard furnace tests to determine their 'fire resistance' [3]. In these tests, isolated full-scale building elements (e.g., walls, slabs, beams, columns, doors) are tested under the exposure of a prescribed heating regime (referred to as a 'standard fire'), which is typically defined by a nominal time-temperature curve. Even if the goal of this harmonised framework is to systematically assess, compare and classify various building elements, the engineering and research community has been repeatedly stressing the high temporal and economic costs associated with these tests [4]. In addition, standard furnace tests inevitably face challenges concerning repeatability and uncertainties related to the thermal boundary conditions (BCs) imposed on test samples. Particularly discrepancies have been reported between various construction materials (e.g., combustible vs. non-combustible) and during the initial testing phases (e.g., the first 10 minutes when many materials undergo important thermal degradation phenomena) [5], [6].

In response to these shortcomings, bench-scale fire testing is becoming increasingly popular for research and development purposes and for studying specific and complex fire-related phenomena. The thermal BCs imposed on test samples are of key importance, and bench-scale experimental setups aim at having them well-defined and highly repeatable [7]. The careful control of the thermal BCs on test samples is usually achieved by specifying a radiant heat source and specific geometry (i.e., view factor), thus controlling the radiative heat flux, according to Stefan-Boltzmann's law [8]. Many experimental setups and standard test methods involve gas-fired radiant panels, like the Lateral Ignition and Flame Spread Test (LIFT) [9], [10] and the Heat-Transfer Rate Inducing System (H-TRIS) test method [11]. Gas-fired radiant panels offer a radiant heat source of high and stable temperature, enabling the achievement of high and well-characterised heat fluxes on test samples.

It is important to recognize that setups like radiant panels are not supposed to act as a substitute for standard fire tests because they have a different purpose. Standard fire tests are primarily used for ensuring compliance with building codes and regulations (e.g., [12]), whereas bench-scale scale

setups are mostly used in performance-based designs, alternative solution assessments, scientific studies, and product research & development. In this regard, setups like radiant panels bring a high degree of flexibility and modularity, allowing for a broad range of applications with excellent control over the thermal BCs, making it ideal for scientific studies such as in [13], [14]. Thus, such setups serve as an additional tool that allows for specific test designs, tailored to evaluate the parameters of interest, which can in turn be used for model development. Amongst others, this means that reaching the maximum heat fluxes that can be obtained in natural fires is not necessarily the primary target for bench-scale setups like radiant panels. Rather, the primary targets are their ease of use and well-controlled thermal BCs.

Established applications of radiant heaters include the cone calorimeter, the Fire Propagation Apparatus (FPA), and LIFT. The cone calorimeter is employed to study the flammability parameters of small samples including time to ignition, heat release rate, effective heat of combustion, mass loss rate, gas toxicity, and soot production. In this setup, radiative heat flux is generated by electric coils positioned above the sample [15]. The FPA is used to assess flammability characteristics under various airflow conditions, utilizing carbon dioxide generation and oxygen consumption calorimetry to determine heat release rates [16]. The radiative heat flux is imposed by halogen lamps surrounding the specimen. LIFT measures flame spread rates under controlled conditions, using gas-fired radiant panels to produce a well-controlled heat flux [17]. While these devices operate on the same fundamental principle, they differ in implementation. The gas-fired burner technology from LIFT can reach the highest heat fluxes but lacks rapid adjustability. The electric coil system of the cone calorimeter is capable of reaching approximately 100 kW/m² [15], which is a desirable value for fire testing [15], but also has limited heat flux adjustability speed due to the high thermal inertia of the electric coils. In contrast, the halogen lamps of the FPA have the potential for rapid heat fluxes adjustment, but they can typically reach lower heat fluxes (approximately up to 65 kW/m²) [18], which is significantly lower than the other methods. The radiant panel technology with ceramic heaters is yet another type of technology, which can reach relatively high heat fluxes (up to 140 kW/m² after long heating in [19]), but also lacks rapid adjustability.

The H-TRIS apparatus combines the powerful gas-fire radiant panels of the LIFT with a dynamic control of the panel positioning (view factor) to rapidly adjust the heat flux. It has been developed at the University of Edinburgh and has had much success in the past decade [11]. The system typically employs an array of gas-fired radiant panels to impose various time histories of radiative heat flux [11], [20]. The thermal BCs imposed on test samples are carefully characterised by controlling the

relative distance between the exposed surface of the test samples and the radiant panel array, which is mounted on a computer-controlled linear motion system. Thus, the precise BC control is achieved by a real-time adjustment of the view factor. This methodology has been adopted by many research and engineering teams around the world. Amongst other applications, H-TRIS has been used to investigate fire-induced explosive spalling in concrete [21]-[23], the fire protection performance of swelling intumescent coatings [24]-[29], the behaviour of glass systems and structural elements[30], wooden and timber structural elements [31], and thermal insulation materials [32], when exposed to elevated temperature and fire conditions. The H-TRIS setup is however necessarily limited by the facilities in place for moving the panel (a vertical H-TRIS setup is not easily adjusted to a horizontal setup). Even if many fire laboratories successfully adopted testing methodologies involving gas-fired radiant panels, other laboratories found it difficult due to challenges related to gas supply and safety, workplace health and safety concerns related to the release of combustion products and smoke, the unavailability of an exhaust hood, and the associated costs [19]. Also, traditional gas-fired radiant panels still present challenges, the most important being the limitations to rapidly adjusting to strongly variable heat fluxes, and an inability to easily adjust the panel orientation. As a consequence, various researchers have been looking into developing alternative solutions to create heat sources/surfaces of high and stable temperatures. Recent attempts involved electricity-powered radiant panels, for instance using ceramic heating pads [19], [33], [34]. However, these solutions faced important constraints due to the relatively low operating temperatures, limiting the range of possible heat fluxes to be imposed on test samples, uncertainty in thermal BCs and high thermal inertia, which limits the application range to slowly changing heat fluxes.

Consequently, there remains a need for a technology that can achieve high heat fluxes (around 100 kW/m^2) while enabling rapid adjustments in heating conditions. The present study attempts to fill this gap by presenting an innovative apparatus for fire performance testing, namely the High-Intensity Fast-Response Electric radiant Panel (HIFREP). This apparatus is powered by electricity and employs high-temperature emitters similar to the FPA to impose well-defined and highly repeatable thermal BCs through a radiative heat flux. It avoids the direct combustion of gas, allowing its use on non-combustible materials in traditional structural testing laboratories that are not equipped with classical fire lab facilities (e.g. high-pressure gas lines and exhaust hoods). Additionally, it can quasi-instantaneously modify heat fluxes by adjusting the input voltage, which in turn modifies the current across the emitters. The time constant of the emitters has been found to be less than 1 s both during heating and cooling, as demonstrated in section 3.6. This makes the apparatus very well-suited for

scientific work, such as the validation of FEM simulation results in the context of structural fire engineering.

In the first part of the paper, the different components of the panel and their importance in the overall setup are discussed in detail. Subsequently, the specifications of the panel's output are discussed through a heat flux calibration. Lastly, the performance of HIFREP in a real test is demonstrated.

2 RADIANT PANEL DESCRIPTION

2.1 Overview

The HIFREP is engineered to impose well-controlled and repeatable thermal BCs on test specimens. These BCs are specified by a time history of radiative heat flux generated by electrically powered emitters. The HIFREP setup and its components are depicted in Fig. 1. The emitters and their electrical connections are housed within a stainless steel module, which is in turn fastened to a mounting steel frame. This mounting frame also supports the terminal box of the HIFREP, the ventilation system for cooling, and other essential control components. The mounting frame is equipped with L-shaped steel profiles (8 cm by 8 cm) to enable the horizontal or vertical positioning of the panel on a rolling steel support structure. The subsequent sections provide a detailed description of the entire setup and the critical components of the HIFREP. The entire setup, including the electrical system, was designed by Weiss Technik with a branch in Liedekerke, Belgium.

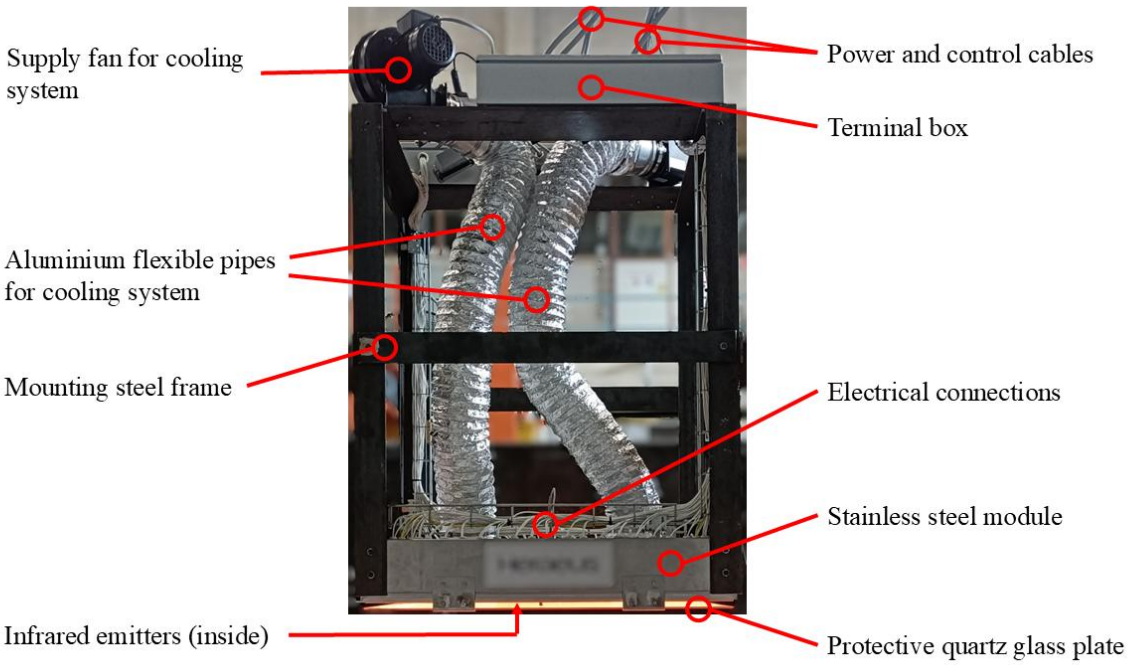

Fig. 1 Picture with an overview of the radiant panel setup components

2.2 Infrared emitters

The HIFREP incorporates 21 densely arranged short-wave emitters with a length of 700 mm (with 500 mm designated as the heated length). Each emitter consists of two electrically separated Tungsten heating filaments enclosed within a protective quartz glass tube. The emitters are spaced at regular intervals of 40 mm (leaving a 17 mm gap between the emitters), creating a rectangle of 900 mm by 500 mm. The rear surface of the glass tube is coated with a reflective quartz layer, effectively directing all radiation towards the front of the panel. Fig. 2 provides a close-up showing the emitters. This infrared emitter technology is typically applied in industrial heating and drying processes. For the manufacturer, the novelty of HIFREP is the density at which the emitters have been arranged, which is much higher than in regular applications and therefore puts challenges on the appropriate cooling of the emitters.

Fig. 2 Illustration of radiation emitters operating at low intensity

The radiative heat flux is generated by an electric current through the Tungsten filaments, causing them to heat up and emit radiation. At maximum operating temperature, the manufacturer specifies radiation within a wavelength range between 0.3 and 5 µm, with a peak at approximately 1.1 µm, as detailed in Fig. 3. The emitted radiative heat flux can be precisely regulated by adjusting the current through the filaments, and therefore their operating temperature. At lower operating temperatures, the peak of the emission spectrum will shift to higher wavelengths, according to Wien's displacements law [35], but this information has not been provided by the manufacturer. Due to the emitters' low thermal inertia, changes in the supplied current result in quasi-instantaneous adjustments in the radiative heat flux. At the emitter level, the radiative heat flux can reach up to about 200 kW/m², while values around 100 kW/m² can be expected in the middle of the panel at 10 cm distance. The

incident radiative flux naturally reduces with increasing distance from the emitters. Detailed specifications on the radiation intensity and the resulting heat fluxes are provided in Section 3.2.

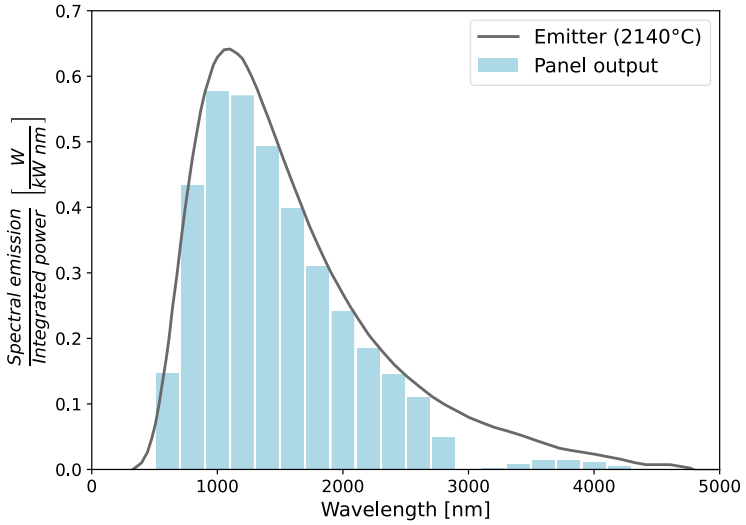

Fig. 3 Spectral emission of an emitter in isolation at maximum operating temperature (Emitter (2140 °C), data provided by the manufacturer) and the panel output taking into account absorption by the protective quartz glass plate (spectral transmissivity provided by the manufacturer). The panel output is the multiplication of the spectral emissivity of the emitter and the spectral transmissivity of the glass plate. Additional radiation from the glass once heated is not considered

2.3 Protective quartz glass plate

The stainless steel module housing the emitters is designed to accommodate a protective quartz glass plate in front of the emitters (see Fig. 1). This glass plate's primary function is to safeguard the emitters from unexpected occurrences during testing, such as mechanical impacts from concrete fragments and falling debris. Nevertheless, the presence of this protective quartz glass reduces the heat flux received by the specimen by 10 to 15%. These values have been determined based on the multiplication of the spectral transmissivity of the glass plate and the spectral emissivity of the emitters, both as specified by the manufacturer, and have been confirmed by measurements. The influence of the protective quartz glass plate on the emission spectrum at maximum operating temperature is visible in Fig. 3, in particular on wavelengths above 2800 nm. It should, however, be noted that the change in emission spectrum at lower temperatures due to Wien's displacement law, implies that the effect of the protective quartz glass will also alter. The protective quartz glass can be removed if wanted.

2.4 Power supply

An electric cabinet facilitates the system's power supply. Herein, the three-phase current, tapped from the general electricity grid by a 5-pin industrial connector, is converted into a direct current (DC), which is then supplied to the terminal box of the HIFREP by industrial connectors. The power supply was designed as an integral part of the entire panel setup and hence meets all the relevant Belgian standards regarding health and safety. Operating at maximum capacity, the system has a power output of 90.9 kW and the voltage over the emitters is 400 V. The energy cost of operation depends on the energy price, the intensity level and the duration, but the kWh cost of a single test with a duration of up to 2 hours can be estimated in the order of magnitude of tens of euros. With a view to sustainability, it is worth noting that the building which hosts the panel has been fitted with extensive arrays of PV panels. The power supply is equipped with two levels of protection based on the temperature in the stainless steel module of the emitters. The first safety level activates an alarm at 50 °C, alerting the operator, while the second level triggers a complete shutdown of the panel at 80 °C.

2.5 Cooling system

While HIFREP is engineered to impose a heat flux on test specimens equivalent to fire exposure, it is essential to maintain a relatively cool operating temperature to prevent damage to its components. This is achieved through an air-cooling system comprising two fans drawing ambient air. The air is directed to the stainless steel module and the emitters via aluminium flexible pipes, cooling all components (see Fig. 1). A perforated steel plate situated behind the emitters ensures the air cooling stream is evenly distributed. After cooling the emitters, the air stream is deflected sideways by the protective quartz glass plate at the front of the panel. This strategic deflection minimises the impact on the convective flows around exposed specimens.

The cooling fans and piping are secured to the mounting steel frame, with the fans positioned sufficiently far from the panel to ensure the air intake is sourced from a region with a reasonably low temperature. This prevents a 'flow short circuit' caused by hot air around the stainless steel module and its emitters.

2.6 Control system

The HIFREP setup is managed by a custom-developed graphical user interface (GUI) programmed in Python, allowing for intensity control from 0 to 100%. This intensity setting is communicated to the power cabinet via a 0-10 V voltage signal, which the panel then converts into the current passing

through the emitters. This operation mode, combined with the emitters' low thermal inertia as mentioned in Section 2.2, enables quasi-instantaneous (as quantified in Section 3.6) and precise adjustments of the imposed thermal BCs. Changes in input intensity are quasi-instantaneously reflected in the radiative intensity, ensuring accurate control of the incident radiation.

The control system also monitors a freely positioned heat flux gauge. Ideally, this gauge is placed in the same plane as the exposed surface of the test specimen to accurately record the time history of imposed heat fluxes during testing. While the radiant panel is designed to provide radiative heat flux, natural convection effects may affect the heat flux, notably when the specimen is located very close to the panel [20].

Finally, during exposure, the protective quartz glass plate heats up and emits radiation, affecting the heat flux as received by the specimen. To address this, the custom-developed GUI is equipped with a feedback loop that adjusts the total imposed heat flux to the desired level, ensuring accurate control throughout the testing process.

2.7 Safety

Any user of HIFREP or similar should develop a Standard Operating Procedure (SOP) and a safety protocol when testing at high temperatures. A specific feature of HIFREP is the high light intensity when operating at high intensity. Therefore, protective eyewear is recommended when the panel is operated.

3 CALIBRATION

3.1 Calibration procedure and instrumentation

The radiant panel calibration process consists of two parts. First, the spatial distribution of the radiative heat flux is assessed by measuring heat fluxes over $1/4^{th}$ of the panel. Heat flux maps for the entire panel in horizontal orientation are then obtained by employing symmetry. In the second phase, the linear scaling of the heat flux with the panel output intensity and the time constant of the panel are assessed, the symmetry of the panel in horizontal orientation is confirmed, and the results are compared with measurements in vertical position.

The current calibration focuses on the radiative heat flux shortly after the panel is turned on. When the panel is operated for a longer period, the protective quartz glass plate will heat up, resulting in an additional radiative heat flux on the exposed surface of a specimen. The temperature of the protective

quartz glass plate, however, depends on the operating time, the panel's intensity, the temperature of the exposed surface of the tested specimen and the configuration of the test. Therefore, it is inherently case-dependent. The effect of the glass plate cannot be avoided, but by limiting the operating time, its effect remains limited. Similar findings for gas-fired radiant panel arrays have been reported in [20]. Convective heat transfer is also case-dependent as it depends on the surface temperature of the specimen, on its size (altering the convective heat transfer coefficient), and on the orientation. Besides, the heat flux gauge is positioned in isolation and is kept cool (water-cooled), limiting convective heat transfer. Consequently, the only heat flux that can be calibrated is the direct radiative heat flux from the emitters. As radiation is independent of the orientation, there should not be a noticeable difference between the calibration results in horizontal and vertical positions. This hypothesis (no difference between horizontal and vertical positions) will be verified later on.

The calibration measurements employ a water-cooled Schmidt-Boelter-type heat flux gauge. The gauge is oriented perpendicular to the panel and is fixed to a steel tube, mounted on a stand to maintain the desired orientation, as depicted in Fig. 4. The heat flux sensor has a resistance of 26.5 Ω and is specifically designed to measure heat fluxes above 5 kW/m². The operational range extends up to 200 kW/m², and it exhibits a calibration uncertainty of 5.9%, which corresponds to a level of confidence of 95%, measured under reference conditions of 100 kW/m² [36].

Fig. 4 Heat flux gauge positioning during HIFREP calibration

Ideally, the sensor's output voltage varies linearly with the received heat flux. Deviations from this linear behaviour are captured in the non-linearity-related uncertainty, expressed by the manufacturer as a percentage of the measurement range. For the employed heat flux gauge, the non-linearity specification amounts to ± 2% of the measurement range. Given that the measurement range extends up to 200 kW/m², the non-linearity-related uncertainty contributes 4 kW/m² regardless of the measured value. The relative magnitude of this error will thus be significant at low intensities [36].

3.2 Heat flux maps

The first phase of calibration involves 24 heat flux measurement positions. The measurement grid layout is depicted in Fig. 5, illustrating a 100 mm spacing between adjacent measurement locations. The positions are accurate to ± 1.0 cm. Radiation intensities of 10%, 50% and 100% of the panel's maximum capacity are imposed. The measurements are conducted at distances equal to 5, 10, 15 and 20 cm (± 0.2 cm) from the protective quartz glass plate. The panel is positioned horizontally, facing downward, to reduce the influence of the convective flows induced by the panel's cooling system. In the vertical position, the cooling airflow in the panel would be partially directed downwards, impinging on the floor and then entering the area of the heat flux gauge. In the horizontal position, the cooling air stream can be diverted horizontally, limiting its influence on the heat flux gauge.

During the design stages of HIFREP, it was decided to have a zone of uniform heat flux of 70 cm by 30 cm in the centre of the panel. Even though many of the measuring positions of Fig. 5 fall outside the zone of uniform heat flux, they provide relevant information for characterizing the exposure of larger test samples where the exposure outside the main target area may influence the overall response, e.g., through its effect on the heating of a structural element and associated deformations.

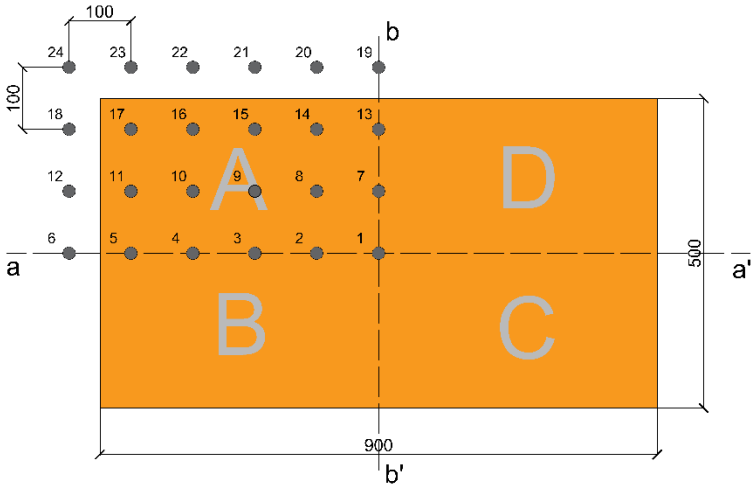

Fig. 5 Measurement positions for the spatial distribution of the heat flux in the exposed area (distances in mm). Measurement position 1 is located directly underneath the centre of the radiant panel

To avoid heating of the protective quartz glass plate, the panel is only turned on for a short time, in which the heat flux-time history is recorded. The calibrated value of the heat flux will be based on the derivative of the heat flux-time history (rate of change). Specifically, the calibrated value of the heat flux is determined as the value at which the rate of change drops below 10% of the maximum rate of change. For this purpose, the data is first disposed of outliers. Subsequently, the data is smoothened using a moving average approach with a window of 0.5 s to eliminate white noise. A visual representation of the approach is provided in Fig. 6, which limits the visualized time frame to the first 25 s for clarity. It should be noted that this procedure works well for heat fluxes that are significantly higher than the magnitude of the noise, which is independent of the operating intensity as it is determined by equipment and cables. Larger uncertainties on the calibrated value of the heat flux can thus be expected for low heat fluxes – resulting from the low operating intensity and/or view factor – because for these situations the magnitude of the uncertainty on the heat flux measurement is comparable to the magnitude of the noise.

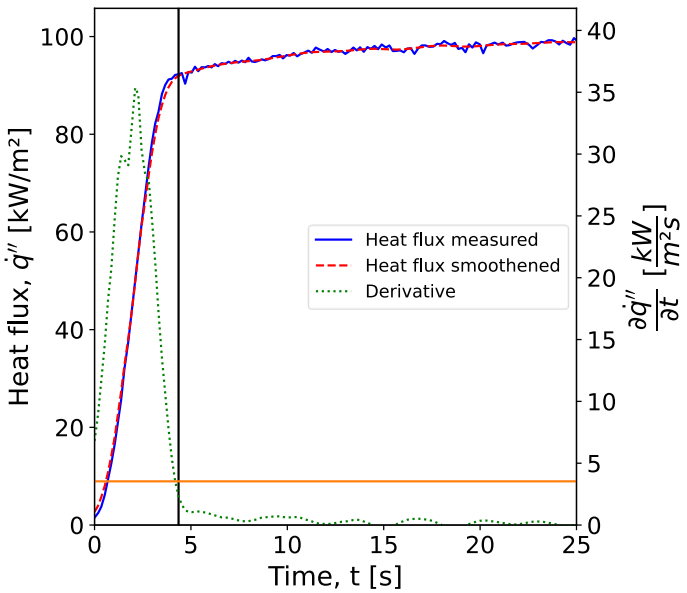

Fig. 6 Example of calibration procedure showing the measured heat flux, smoothened heat flux and the derivative of the smoothened heat flux. The visualized timeframe is limited to the relevant times for understanding the calibration methodology

The heat flux maps from the calibration measurements in quadrant A (see Fig. 5) are combined using symmetry to generate a complete radiative heat flux map for the entire panel. The resulting heat flux maps of Fig. 7 correspond to distances of 10 cm and 20 cm from the protective quartz glass plate, considering intensities of 10%, 50% and 100%, respectively.

The presented heat flux maps reveal a region characterized by relatively uniform heat flux at the central portion of the panel, spanning approximately 70 by 30 cm, as was specified in the technical discussions with the manufacturer. The minimum, maximum and average values as well as the standard deviation of the measured heat fluxes in this zone are provided in Table 1. This area is indicated by a cyan rectangle in Fig. 7, compared to the radiative surface of the panel (i.e. emitters) depicted with a red rectangle. Close to the panel, at a 5 cm distance and maximum intensity, the heat flux within this operation zone reaches a maximum value of 105 kW/m². At a distance of 10 cm, the maximum heat flux amounts to about 92.5 kW/m², as shown in Fig. 7e. The heat flux reduces towards the edges of the panel due to a reduction in the view factor and also decreases with panel output intensity. The spatial variations in heat flux, as delineated by the heat flux maps, allow to design test setups which impose specified thermal BCs on tested specimens.

Table 1 Minimum, maximum, and average heat flux with standard deviation in the zone of uniform heat flux specified by the manufacturer. The values are based on the actual measurements in this zone

	10 cm distance				**20 cm distance**			
Intensity	$\dot{q}''_{min}$ [kW/m²]	$\dot{q}''_{max}$ [kW/m²]	$\mu_{\dot{q}''}$ [kW/m²]	$\sigma_{\dot{q}''}$ [kW/m²]	$\dot{q}''_{min}$ [kW/m²]	$\dot{q}''_{max}$ [kW/m²]	$\mu_{\dot{q}''}$ [kW/m²]	$\sigma_{\dot{q}''}$ [kW/m²]
10%	6.6	7.4	7.0	0.4	4.6	5.4	5.0	0.3
50%	37.2	42.6	40.4	2.3	29.9	30.0	30.0	2.4
100%	77.4	89.0	84.2	4.9	54.2	66.9	60.9	5.2

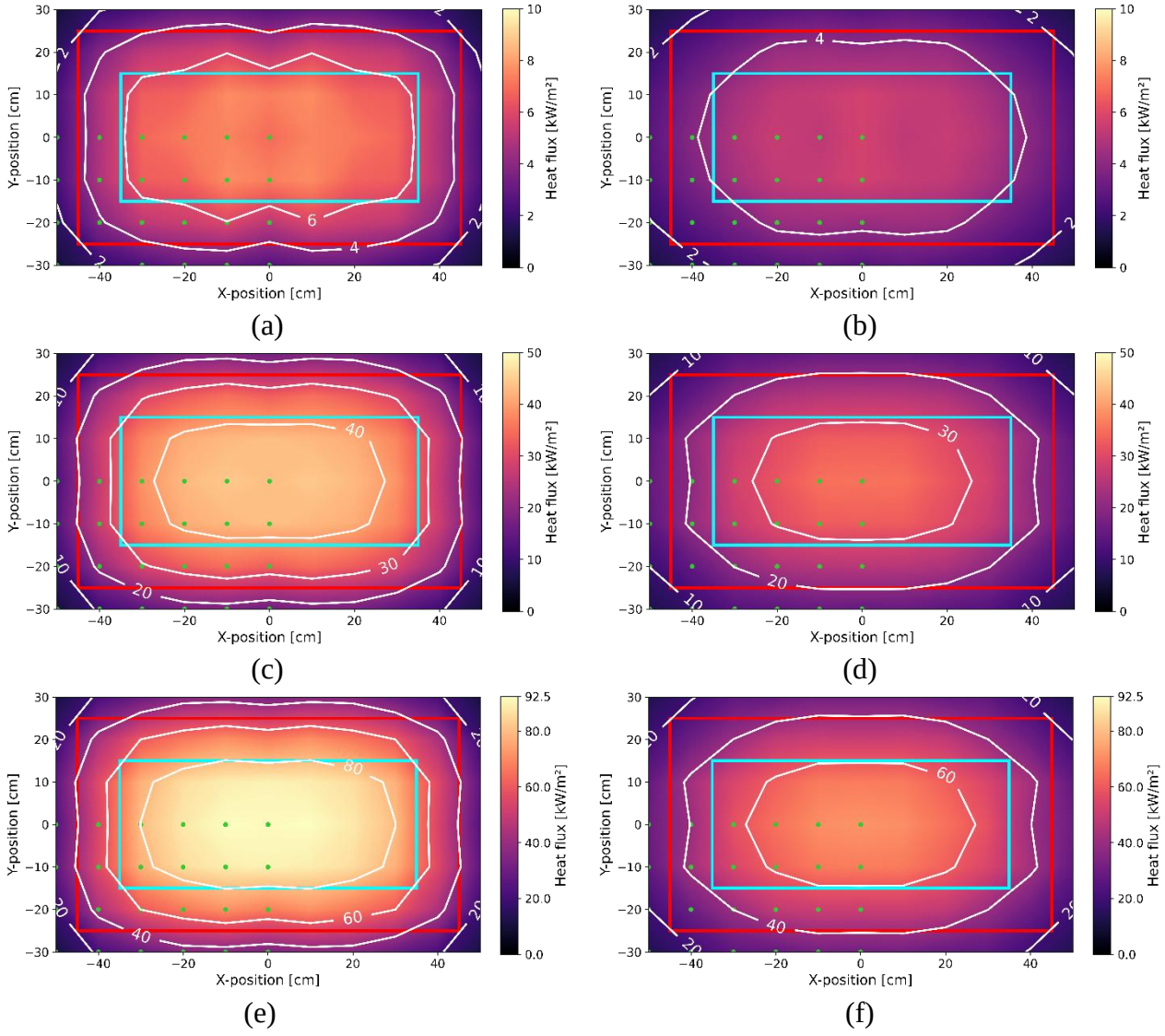

Fig. 7 Heat flux maps at (a) 10 cm and 10% intensity, (b) 20 cm and 10% intensity, (c) 10 cm and 50% intensity, (d) 20 cm and 50% intensity, (e) 10 cm and 100% intensity and (f) 20 cm and 100% intensity. Note the differences in

maximum heat flux in the legends. The red and cyan rectangles indicate respectively the contours of the radiative surface of the panel and the target zone of uniformity, while the green dots represent measuring positions

3.3 Deviation from theoretical calculations

The spatial distribution of the measured heat fluxes can be compared to the spatial distribution as would be expected from the view factor for a rectangular radiant panel surface with uniform radiation intensity. The view factor maps are provided in Fig. 8a and b for distances of 10 and 20 cm respectively. The performance of the panel as compared to the theoretical calculations assuming a plate at uniform temperature as the source of radiation is provided in Fig. 9. The theoretical view factor values are compared with the measured heat fluxes. If the panel could be considered as a plate at a uniform temperature, the measured heat fluxes should be perfectly proportional to the theoretical view factor. The results in Fig. 9 show that although there is a global trend of proportionality, single points may deviate from this ideal behaviour and that the deviations are larger closer to the panel and for lower heat fluxes and view factors. The points inside the cyan rectangle – the target zone for tests – do not deviate significantly from the ideal behaviour. The discrepancy between the theoretical and experimental results is primarily caused by the assumption of a rectangle with a uniform emission power per unit area. In reality, the panel consists of distinct line emitters, covered with a quartz glass coating at the back side to increase reflection and thus radiation to the front side of the panel. The resulting spatial radiative heat flux distribution thus diverges from a rectangle at a uniform temperature. In addition, the protective quartz glass plate also has an influence as it refracts the incident radiation. This underlines the importance of proper calibration through experimental campaigns, rather than relying on theoretical calculations.

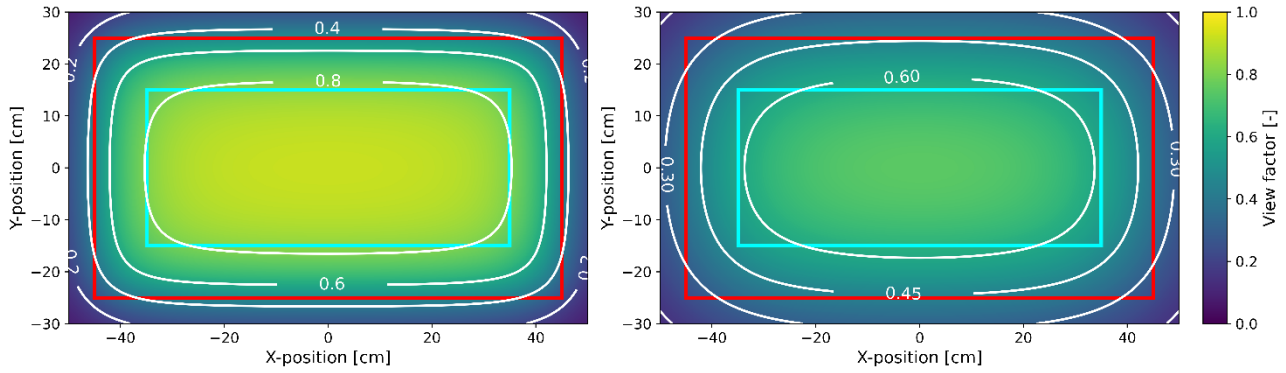

(a) (b)

Fig. 8 View factor map based on theoretical calculations assuming the panel to be a plate at the position of the glass plate and at uniform temperature for distances of (a) 10 cm and (b) 20 cm

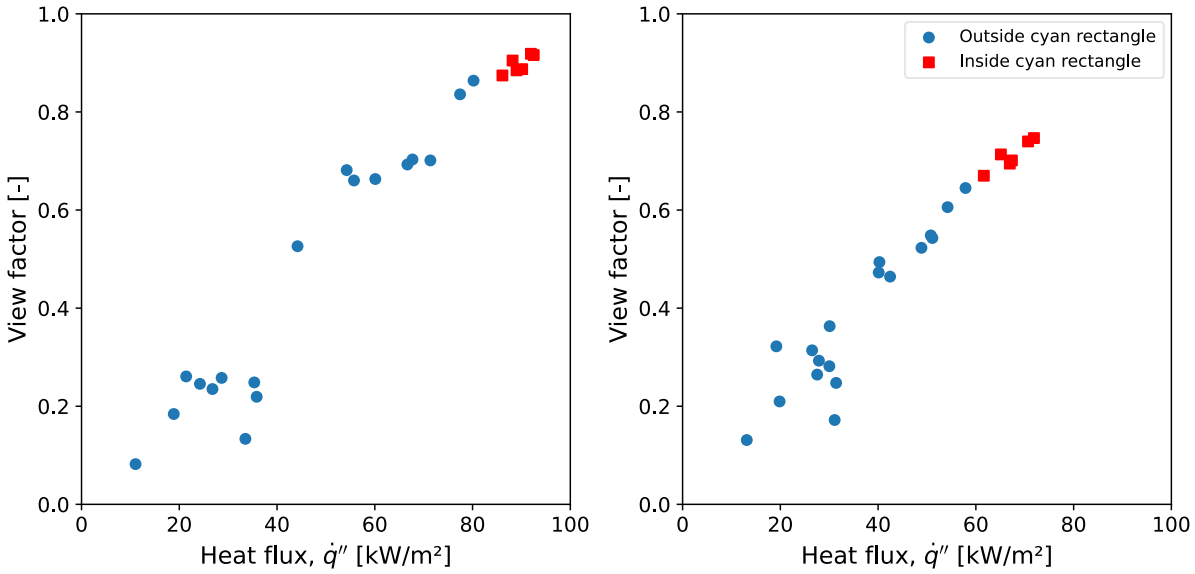

(a) (b)

Fig. 9 Comparison of measured heat flux with theoretical view factor at (a) 10 cm and (b) 20 cm distance at 100% intensity, distinguishing between points inside the cyan rectangle (zone of 'uniform' heat flux) and the points outside the cyan rectangle

3.4 Panel symmetry

To confirm the symmetry of the panel, additional measurements have been performed on the other panel quadrants (B, C and D in horizontal orientation, and A, B, C and D in vertical orientation, see Fig. 5). These additional measurements are processed in the same way as the initial measurements and the results are compared with the original results. The additional measurement positions are given in Fig. 10 and were chosen to be inside the operation zone as tests are primarily performed in this zone. Outside this zone, high heat flux gradients can be encountered, as demonstrated in Fig. 8, and small deviations in positioning (estimated to be up to 1 cm accurate) can lead to significant differences in measured heat flux.

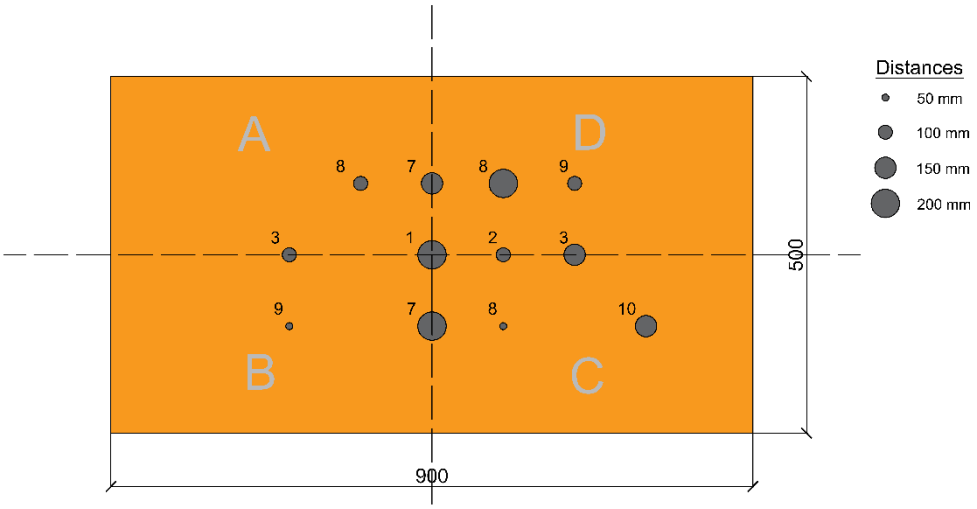

Fig. 10 Additional measurement positions for calibration, measurements in [mm]. The midpoints of the dots indicate the position, using the same numbering as in Fig. 5, while the dot size represents the distance to the protective quartz glass plate

Fig. 11 compares the measured heat fluxes at the positions in Fig. 10 to the measured heat fluxes of the original calibration. The results indicate a very good agreement between the additional measurements and the original calibration, well within the 95% confidence interval. Therefore, the results from the emitter heat flux calibration over 1/4th of the panel in horizontal orientation can be extended to the other quadrants of the panel, both in horizontal and vertical orientation. This result implicitly confirms that the convective heat flux is negligible, which was intended by turning the panel on for short periods only and using the heat flux gauge in isolation.

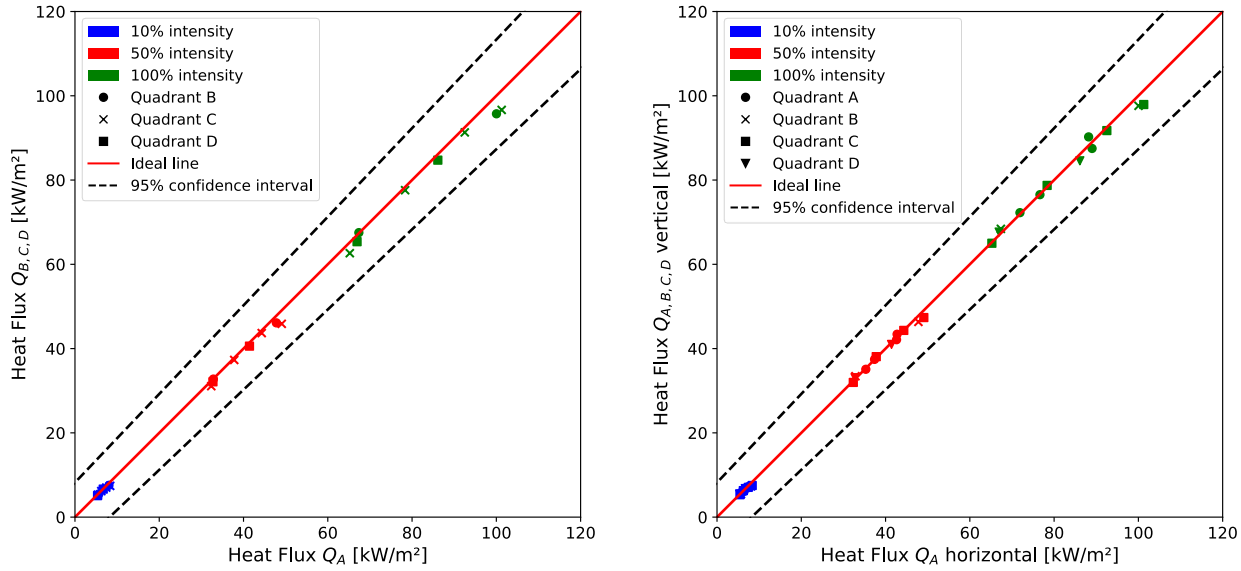

Fig. 11 Assessment of the symmetry assumption for (a) horizontal orientation and (b) vertical orientation

3.5 Linear scaling of heat flux with panel intensity

Utilizing the acquired data from the original calibration in Section 3.2, an assessment of the linear scaling of the measured heat flux with the imposed panel intensity is made. Fig. 12a, Fig. 12b, and Fig. 12c compare the measured heat fluxes between panel intensities of (a) 10% and 50%, (b) 10% and 100%, and (c) 50% and 100% respectively, and confront them with the ideal line, signifying a perfectly linear relationship between measured heat flux and imposed panel intensity. The data points in Fig. 12c are close to the ideal line, with a small rightward deviation for the highest heat fluxes. This deviation is considered to be linked to the heating of the protective quartz glass plate, which causes an additional radiative heat flux. When the imposed intensity is higher, the quartz glass plate will heat up more and the additional heat flux will be higher.

A comparison of the data at 50% and 100% intensity with the data at 10% intensity, as shown in Fig. 12a and Fig. 12b, appears to yield less satisfying results. While a similar trend to Fig. 12c is observed, the rightward shift at higher heat fluxes appears to be more pronounced. However, the difference is exaggerated by the different scales on the y-axis for Fig. 12a and Fig. 12b. As for case (c), the shift to the right can be attributed to the heating of the protective quartz glass plate, which causes higher heat flux measurements at higher intensity levels because the glass plate will heat up more.

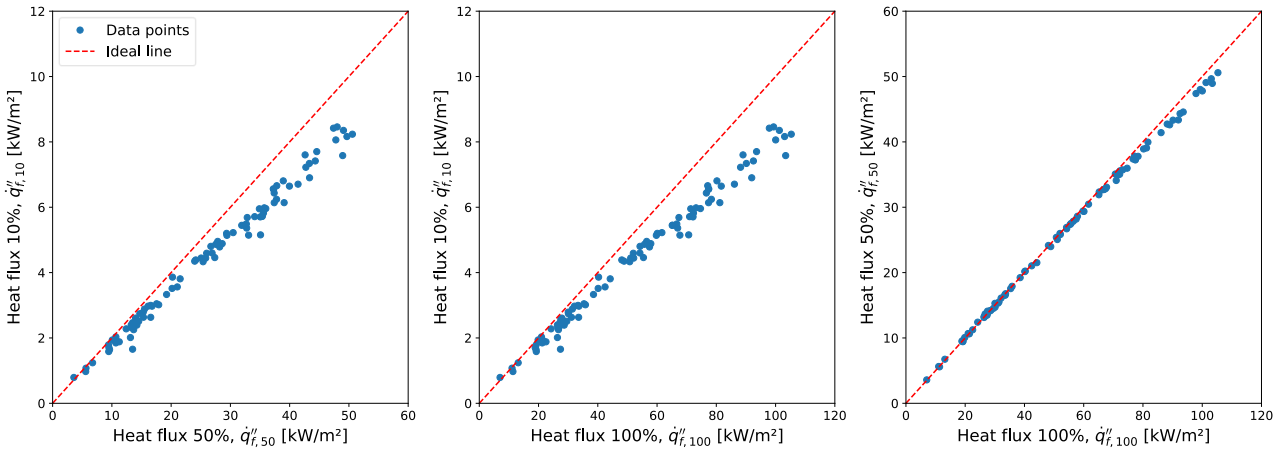

(a) (b) (c)

Fig. 12 Assessment of linear scaling of measured heat flux with imposed panel intensity using the data of (a) 10% and 50%, (b) 10% and 100%, and (c) 50% and 100% panel intensity

The same data has also been combined into a single plot in Fig. 13, which compares the imposed intensity level with the normalized heat flux (i.e., the ratio of the heat flux measured at the imposed intensity level to the measured value at 100% intensity). The results, visualized in boxplots for operating intensities of 10 and 50% indicate a small spread on the results. In addition, the slight

deviation from perfectly linear scaling is confirmed as the ideal, red dashed line passes above the centre of the boxplots.

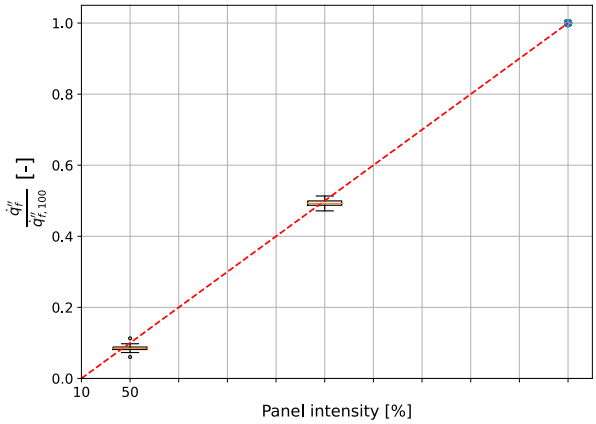

Fig. 13 Assessment of linear scaling comparing the imposed intensity level to the normalized heat flux

3.6 Time constants

The time constant is determined by the slowest reacting component of the system. In the case of the HIFREP, the emitters respond quasi-instantaneously to changes in input, but the protective quartz glass plate responds much more slowly. The time constant of the entire setup is thus determined by the quartz glass plate. To bypass the time constant of the glass plate and to be able to fully harness the quasi-instantaneous response of the emitters, the system has been equipped with a feedback loop, which adjusts the input voltage of the emitters, taking into account the additional heat flux from the protective quartz glass plate.

In order to estimate the time constant of the protective glass plate and the emitters, an additional experiment is performed. First, the panel is turned on at an intensity of 10% for two minutes. Subsequently, the intensity is increased from 10 to 90%, which is maintained for 15 minutes, to let the protective glass plate heat up. Hereafter, the intensity is decreased to 0. The intensity levels and measured heat fluxes as a function of time are provided in Fig. 14. The initial increase in intensity (from 10 to 90%) and ensuing heat flux can be attributed completely to the emitters as the glass plate has not had the time to heat up significantly yet, while the gradual increase hereafter can be attributed to the protective quartz glass plate heating up. Similarly, the sharp decrease in heat flux after the intensity has been set to 0 is due to the emitters cooling down, whereas the gradual decrease hereafter can be attributed almost completely to the protective glass plate, as the time constant of the emitters is much smaller, as will be demonstrated below. The time constant is calculated according to Eq. (1) [37].

$$T = T_\infty - (T_\infty - T_0)e^{\frac{-t}{\tau}} \quad (1)$$

Where T is the temperature [K], T_∞ is the end (or asymptotic) temperature [K], T_0 is the initial temperature [K], t is time [s] and τ is the time constant [s].

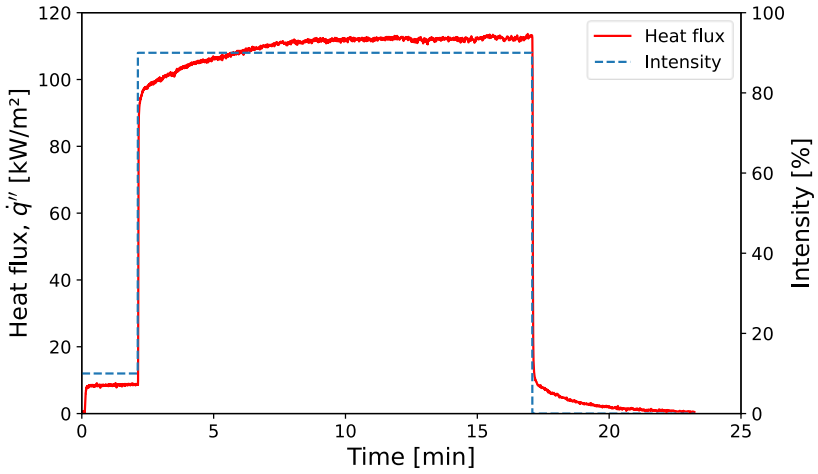

Fig. 14 Imposed intensity levels and measured heat fluxes for the calculation of the time constants

The measured quantity during the experiment is a heat flux, whereas the desired quantity according to Eq. (1) is a temperature. To convert the measured heat fluxes into temperatures, the fourth root of the measured heat fluxes is taken. Theoretically, the emissivity, Stefan-Boltzmann's constant and the view factor should be taken into account, but as they are considered constant, they cancel out in Eq. (1), leaving the fourth root to transfer from the heat fluxes to temperatures.

The results of the regressions during heating are provided in Fig. 15a and Fig. 15b for the emitters and the glass respectively, while the results during cooling are given in Fig. 16. The results indicate that in absolute value the time constant for the emitters during cooling (0.9 s) is considerably longer than during heating (0.5 s). This is, however, not very important as the value for the glass plate is much longer (two orders of magnitude higher), which is almost identical during heating and cooling (respectively 162 and 159 s). Hence, it is the glass plate that determines the overall time constant of HIFREP. In addition, the time constants reveal that it is possible to impose changes in thermal BCs that are slow with respect to the emitters (so they can effectively be assumed in a steady state) and fast with respect to the overall system.

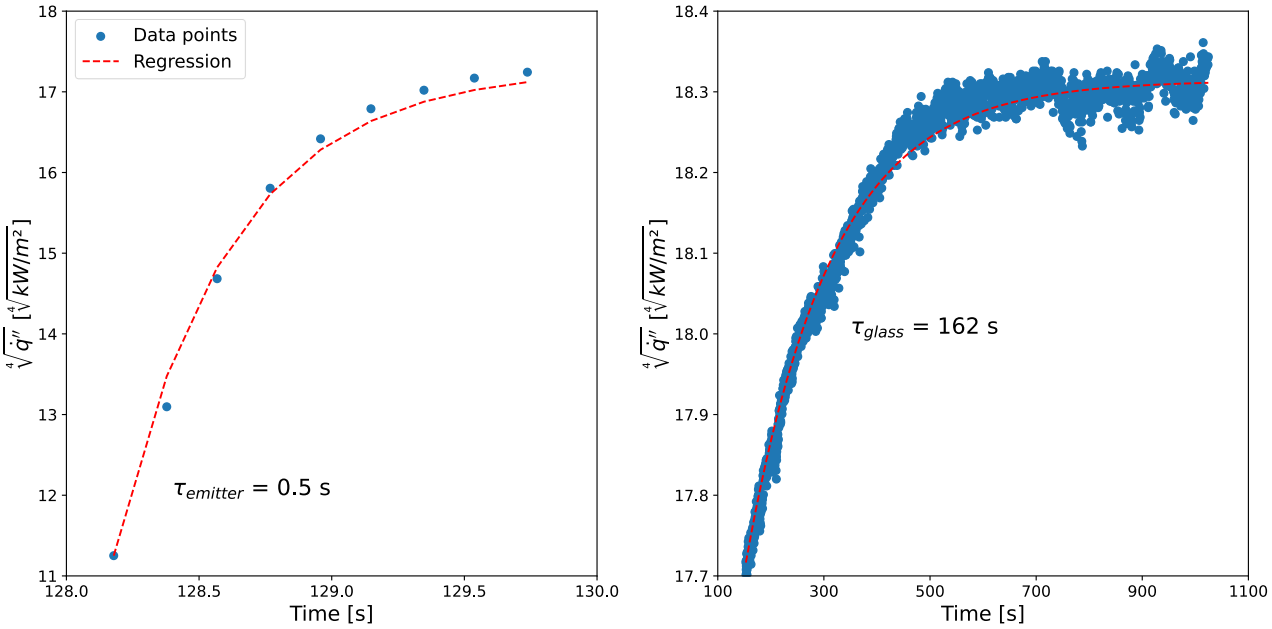

(a) (b)

Fig. 15 Data points and regression during heating for (a) the emitters and (b) the protective quartz glass plate.

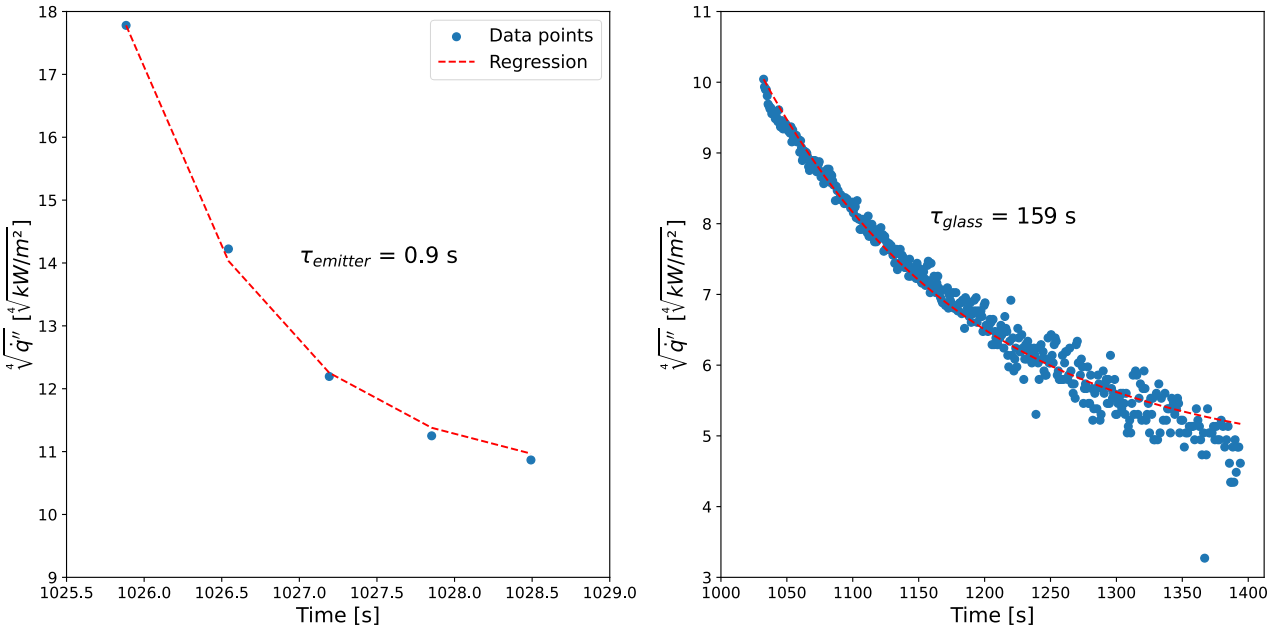

(a) (b)

Fig. 16 Data points and regression during cooling for (a) the emitters and (b) the protective quartz glass plate

4 APPLICATION EXAMPLES

In order to demonstrate the performance of HIFREP, two application examples are provided. The first example considers the heat flux gauge in isolation and demonstrates the ability of HIFREP to

follow an intended heat flux-time history meticulously using exotic target curves. The second application example deals with a realistic experimental setup for structural fire engineering tests.

4.1 Heat flux gauge in isolation

To evaluate the ability of HIFREP to rapidly adjust its output using the PID controller, a challenging target heat flux curve with abrupt changes was applied. To assess repeatability, the same experiment has been conducted three times: twice starting from a cold state (i.e., the panel and quartz glass plate were at ambient temperature: “cold start”) and once from a hot state (the panel and quartz plate were preheated for 5 min at 100% intensity: “hot start”). Fig. 17a shows the comparison between the target heat flux curve and the measured heat fluxes when starting from a cold state, while Fig. 17b shows the comparison of the target with the measurements when starting from a hot state. The results indicate strong repeatability, as the measured heat fluxes closely follow the target heat flux curve in all three cases. Even when sudden jumps in the target heat flux challenge the panel’s performance, the system adjusts its output to the new state within seconds, demonstrating its responsiveness and control accuracy.

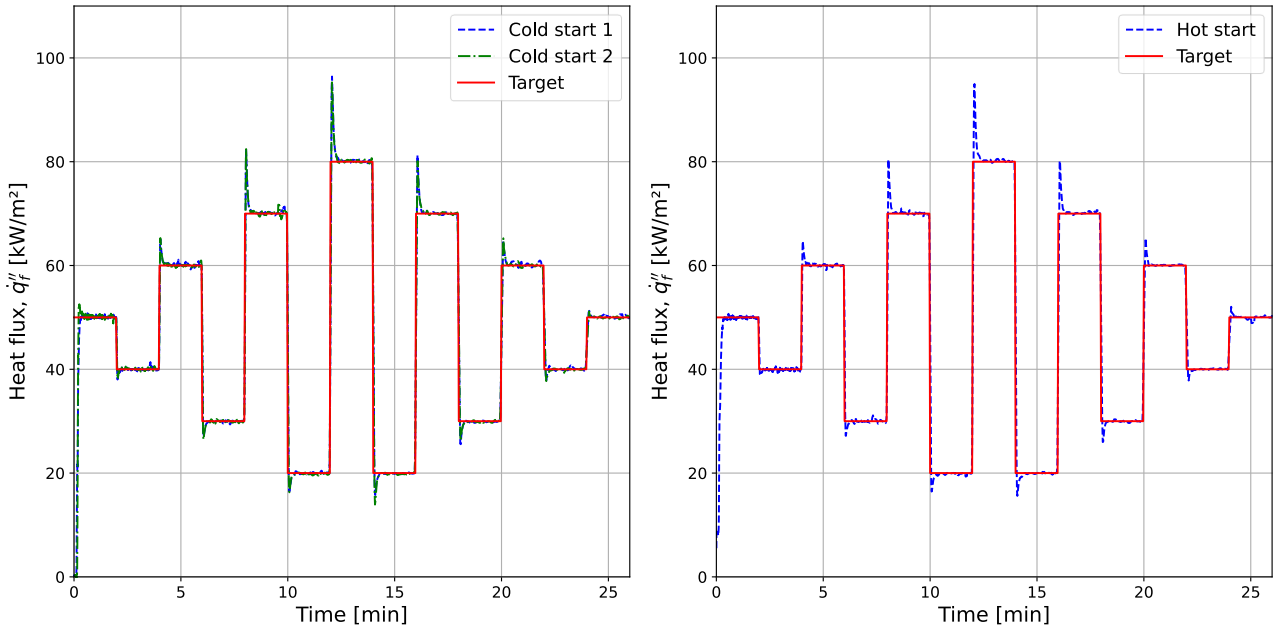

Fig. 17 Comparison between the measured and target heat flux curves when (a) starting from a cold state and (b) starting from a hot state. Measurements were conducted at 10 cm distance from the centre of the panel. The data is smoothened using a moving average approach with a 0.5 s time window

Comparing the imposed intensity levels of the panel during the three tests, shown in Fig. 18, reveals a difference in the panel intensity between the tests starting from cold state on the one hand and the

test starting from a hot state on the other hand. However, this divergence is not noticeable in the heat flux data presented in Fig. 17, confirming that the PID controller effectively compensates for the effect of the protective quartz glass plate. By adjusting the imposed intensity level, the PID controller accounts for the additional heat flux generated by the elevated temperature of the glass plate. This effect is also apparent in the panel behaviour at the constant target values in Fig. 17 (peaks and valleys). At a peak, the imposed intensity level (Fig. 18) slowly decreases over time while the measured heat flux remains stable (Fig. 17), as the heating of the glass plate contributes additional heat flux. Conversely, in a valley, the imposed intensity level slowly increases while the measured heat flux remains constant because the glass plate is cooling down again at these lower intensity levels. The initial discrepancy between the “hot start” and “cold start” tests reduces over time as the starting condition of the panel becomes less important when the glass heats up and cools down over time according to the target heat flux curve. The remaining discrepancies in the panel intensity later in the test are due to differences in the environmental conditions (e.g., ambient temperature).

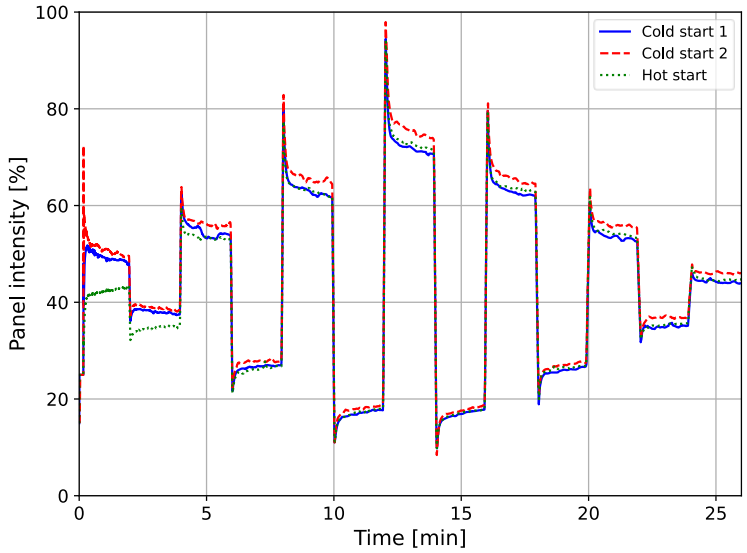

Fig. 18 Comparison in intensity imposed intensity level between the three tests. The data is smoothened using a moving average approach with a 0.5 s time window

As shown in Fig. 18, the imposed intensity level peaks when a sudden shift in target heat flux occurs, and it takes a few seconds for the measured heat flux to stabilize. This is due to the PID controller algorithm currently employed. This is not an issue for application of the panel however, since in realistic fire scenario’s such abrupt changes in heat flux are unlikely. Typically, heat flux varies more gradually over time, allowing the PID system to more easily track the target heat flux. To illustrate this, a sinusoidal function is applied as target heat flux-time history. The comparison between the

imposed target and the measured heat flux in Fig. 19 demonstrates that the PID-controlled system can accurately follow this gradual variation.

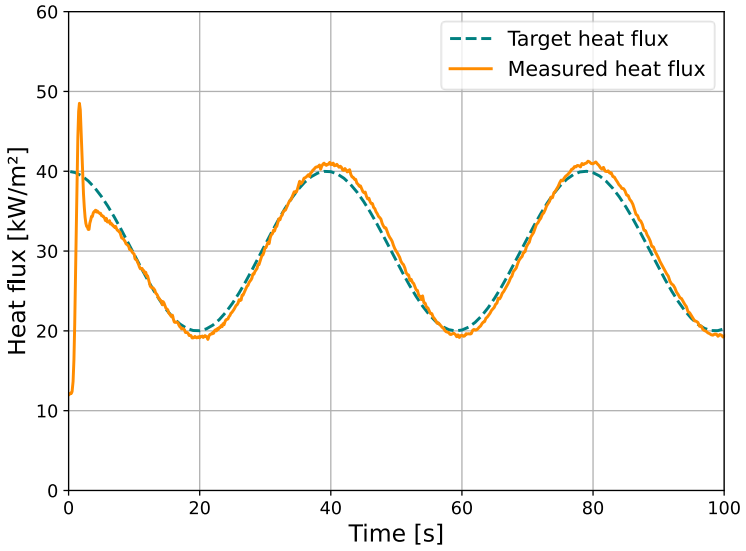

Fig. 19 Measured and target heat flux at 20 cm distance when requesting a sinusoidal intensity level and applying the PID controller.

4.2 Loaded concrete beam burnout performance test

An experimental study has been conducted whereby a loaded concrete beam has been exposed using HIFREP to a natural fire scenario with heating and cooling phases, evaluating the beam's burnout performance. Such burnout performance testing is very challenging using traditional furnaces [38] or existing radiant panel setups, and thus performing such a test using HIFREP constitutes a powerful application case. The temperature measurements in the concrete beam are compared to results from numerical simulations.

4.2.1 Experimental setup

The experimental configuration involved subjecting a reinforced concrete beam with a length of 3.8 m, a width of 0.2 m and a height of 0.29 m to a reversed 4-point bending test (supports in the middle part of the beam and loaded using hydraulic jacks at 20 cm from the sides), which is schematically depicted in Fig. 20 and can be viewed on a photo in Fig. 21. The heated zone was confined to the middle 70 cm of the beam using calcium silicate boards with a thickness of 25 mm to protect the sides and the non-exposed parts. This approach aimed at reproducing one-dimensional heat transfer (although the heat transfer in the beam will be inevitably three-dimensional). The exposure to heat flux at the exposed surface is aimed at following the Eurocode Parametric Fire Curve (EPFC), shown in Fig. 22a, with a heating phase duration of 90 min and a cooling rate of 4.36 °C/min [39]. The test

was stopped after 110 minutes as a steep increase in deformations indicated imminent structural failure of the beam. Thus, the test demonstrated cooling phase structural failure. The EPFC was chosen as a basis for the incident heat flux as the test was performed within the framework of a bigger test campaign which used the EPFC as fire exposure model [40]. Nevertheless, any heat flux-time history (e.g., as derived from OZone) could have been applied for the structural fire tests.

In the following only the thermal response is discussed. Temperatures within the beam were recorded with embedded K-type thermocouples and were continued also after the fire exposure was stopped.

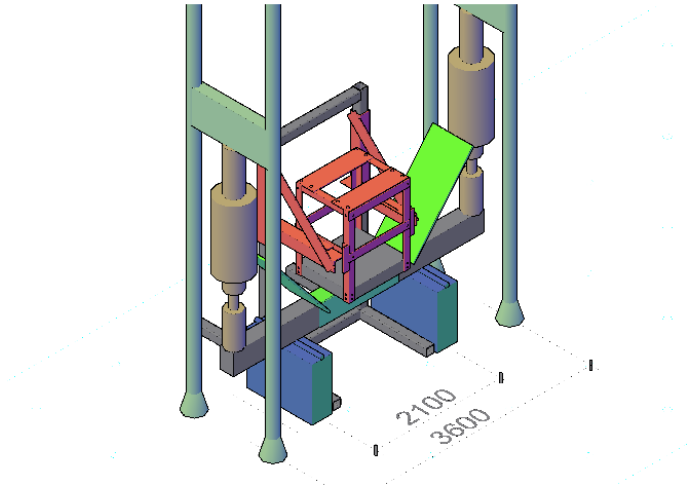

Fig. 20 Schematic view of the reversed 4-point bending setup with the middle part of the beam heated with HIFREP

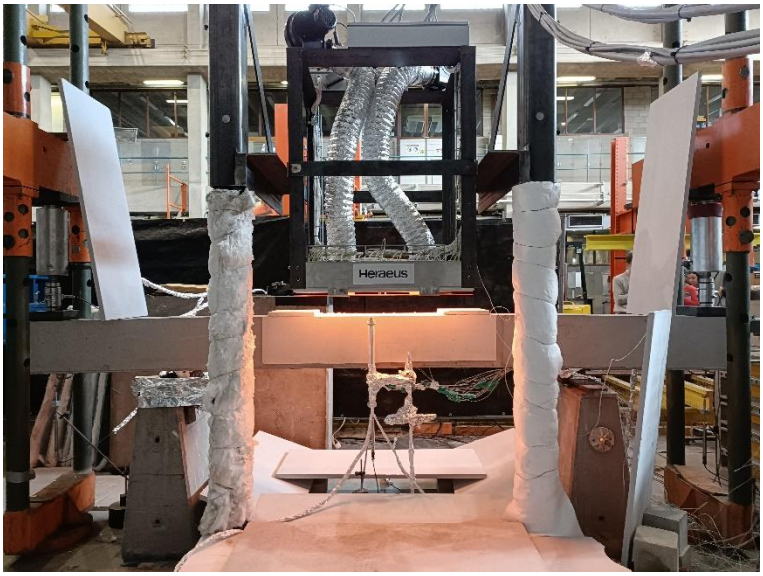

Fig. 21 Photo taken during the initial stages of the test

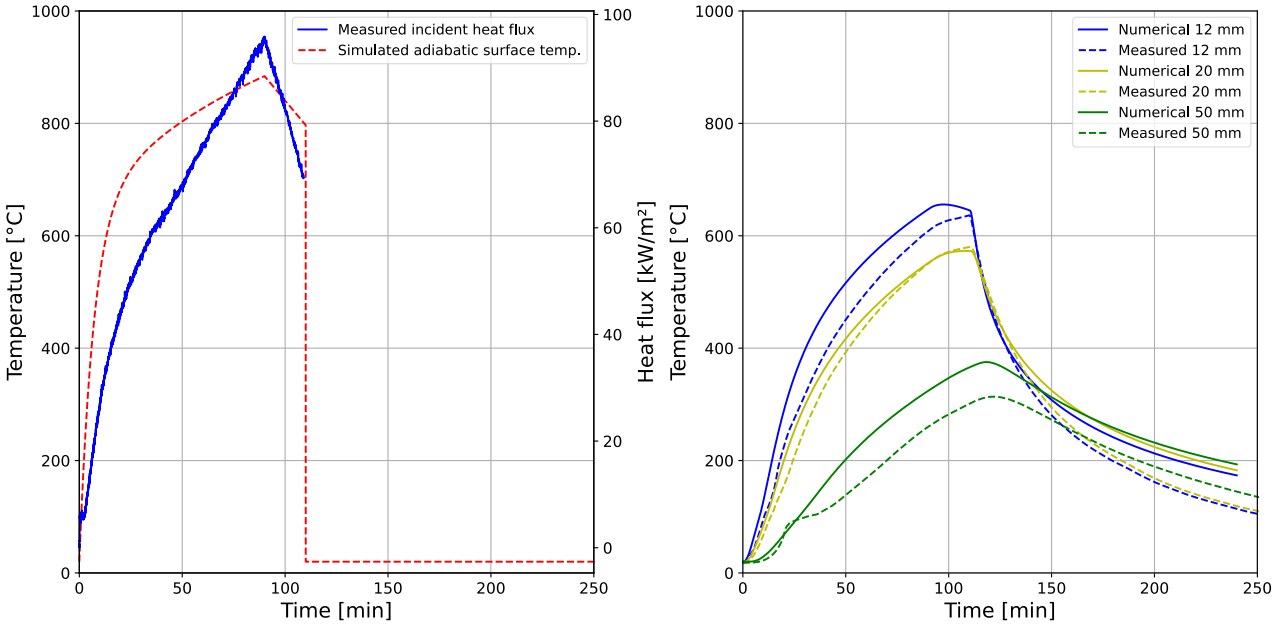

Fig. 22 Temperatures at different depths from the exposed surface as simulated (dashed lines) and recorded during the fire experiment (full lines)

4.2.2 Numerical setup

The finite element analysis is carried out using the software SAFIR [41], version 2019.a.6. The concrete and steel reinforcement were modelled using the materials SILCON_EN and STEELEC2EN respectively, employing the default parameters as stated in EN 1992-1-2: 2004 [12]. The thermal BCs on the top exposed surface, the beam's tensioned side, were modelled as a combination of radiation and convection from an EPFC with a Γ value of 0.45 and a heating duration of 90 minutes. The concrete absorptivity/emissivity was set to 0.7, while the convection coefficient was 35 W/m²K, as specified in EN 1991-1-2:2002 [39] for natural fire exposures. The unexposed sides were exposed to an ambient temperature of 20 °C with an absorptivity/emissivity of 0.7 and a convection coefficient of 4 W/m²K, consistent with the recommendations in [31] and [30] respectively. These EPFC specifications were translated into a panel intensity so that the total heat flux to the surface of the beam would be the same as specified by the adopted EPFC model, see [40].

4.2.3 Analysis of the results

The results are presented in Fig. 22b for three distinct depths from the exposed surface (i.e., 12, 20 and 50 mm). Good agreement between the measured and predicted temperatures can be observed, especially near the exposed surface. The relative differences between the maximum temperatures are 3 and 1.2% at 12 and 20 mm depth respectively. Nevertheless, deviations between the measurements

and the model can be observed. Near the exposed surface, at 12 mm, the deviations may be explained in part by the significant temperature gradient, where minor variations in the thermocouple positioning can lead to significant deviations in the measured temperatures. At 50 mm depth, the deviations are mainly related to the moisture effects (only implicitly considered in the specific heat capacity of concrete), associated with the heat-induced moisture migration.

5 CONCLUSIONS

The High-Intensity Fast-Response Electric Radiant Panel (HIFREP) has been developed as a fire testing apparatus capable of achieving heat flux levels suitable for structural fire testing, reaching values close to 100 kW/m² at 10 cm distance. Additionally, it offers rapid adjustments to the imposed heat flux. Its modularity, ease of use, fast response time, and precise control over thermal boundary conditions make it a versatile tool for a wide range of customized and bespoke experiments. The development of HIFREP is important for the advancement of scientific research, in particular for structural fire engineering, as it allows for the study and evaluation of specific parameters and targets an improved understanding of the behaviour of structural elements under exposure to high heat fluxes.

As HIFREP is fully electric, no combustion occurs on the panel side. Therefore, it can be used in traditional structural testing laboratories, which often do not have the required provisions to deal with the products released by combustion (e.g., extraction hoods), provided that the tested specimens do not contain combustible materials.

HIFREP consists of 21 emitters that allow for a fast, precise and easily adjustable heat flux. The horizontal calibration of the panel revealed that the panel can reach an incident radiative heat flux of approximately 92.5 kW/m² at a 10 cm distance from the protective quartz glass plate. Additional measurements demonstrated that the panel output is independent of its orientation and that the heat fluxes from the emitters scale almost proportionally with the panel intensity. The time constant of the panel is determined by the time constant of the protective quartz glass plate and amounts to approximately 162 s during heating and 159 s during cooling. The integrated feedback loop allows for a bypass of the protective quartz glass plate and harnesses the fast response of the emitters, which have a time constant of around 0.5 s during heating and 0.9 s during cooling.

The main restriction of HIFREP is the limited heat flux that can be produced. In its current configuration, the maximum incident radiative heat flux from the calibration was found to be around 105 kW/m² (at 5 cm distance) with the protective quartz glass plate in place. Besides, the limited exposure area of 700 by 500 mm² prevents the panel from being used in setups of larger scale.

Using the application example of a reinforced concrete beam exposed to a natural fire, it was demonstrated that the HIFREP can be used for structural fire testing considering non-standard fire scenarios. The experimentally measured temperatures in the beam closely matched those of finite element calculations (the difference in maximum temperatures was less than 3% close to the exposed surface), highlighting the ability of HIFREP to be used for research and development in structural fire engineering.

ACKNOWLEDGEMENTS

Florian Put is funded by Research Foundation of Flanders (FWO) within the scope of the research project (Grant number 1137123N) "Characterization of the thermal exposure and material properties of concrete during the fire decay phase for performance-based structural fire engineering". Balša Jovanović is funded by Research Foundation of Flanders (FWO) within the scope of the research project (Grant number 3G010220) "Vibration-based post-fire assessment of concrete structures using Bayesian updating techniques". Dr Lucherini would like to gratefully acknowledge the financial support for the FRISSBE project within the European Union's Horizon 2020 research and innovation program (GA 952395).

STATEMENTS AND DECLARATIONS

The authors declare no conflicts of interest.

DATA AVAILABILITY STATEMENT

Data will be made available upon reasonable request.

REFERENCES

[1] D. Drysdale, *An introduction to fire dynamics*, 3rd ed. Chichester, West Sussex, United Kingdom: John Wiley & Sons, Ltd., 2011.

[2] M. McNamee and B. J. Meacham, 'Conceptual Basis for a Sustainable and Fire Resilient Built Environment', *Fire Technol.*, Sep. 2023, doi: 10.1007/s10694-023-01490-9.

[3] CEN, *EN 1363-1:2020 - Fire resistance tests - Part 1: General requirements*, Brussels, Belgium., 2020.

[4] A. Law and L. Bisby, 'The rise and rise of fire resistance', *Fire Saf. J.*, vol. 116, p. 103188, Sep. 2020, doi: 10.1016/j.firesaf.2020.103188.

[5] D. Lange, J. Sjöström, J. Schmid, D. Brandon, and J. Hidalgo, 'A Comparison of the Conditions in a Fire Resistance Furnace When Testing Combustible and Non-combustible Construction', *Fire Technol.*, vol. 56, no. 4, pp. 1621–1654, Jul. 2020, doi: 10.1007/s10694-020-00946-6.

[6] C. Maluk, 'Motivation, drivers and barriers for a knowledge-based test environment in structural fire safety engineering science', *Fire Saf. J.*, vol. 91, pp. 103–111, Jul. 2017, doi: 10.1016/j.firesaf.2017.05.009.
[7] J. L. Torero, A. Law, and C. Maluk, 'Defining the thermal boundary condition for protective structures in fire', *Eng. Struct.*, vol. 149, pp. 104–112, Oct. 2017, doi: 10.1016/j.engstruct.2016.11.015.
[8] F. P. Incropera, D. P. DeWitt, T. L. Bergman, and A. S. Lavine, *Fundamentals of heat and mass transfer*, 6th ed. Hoboken, NJ: John Wiley & Sons, Ltd., 2007.
[9] ISO, *ISO 9239-1:2010 – Reaction-to-fire tests for floorings – Part 1: Determination of the burning behaviour using a radiant heat source*, Geneva, Switzerland., 2010.
[10] ISO, *ISO 5658-2:2006 – Reaction-to-fire tests – Spread of flame – Part 2: Lateral spread on building and transport products in vertical configuration*, Geneva, Switzerland., 2006.
[11] C. Maluk, L. Bisby, M. Krajcovic, and J. L. Torero, 'A Heat-Transfer Rate Inducing System (H-TRIS) Test Method', *Fire Saf. J.*, vol. 105, pp. 307–319, Apr. 2019, doi: 10.1016/j.firesaf.2016.05.001.
[12] CEN, *EN 1992-1-2: Eurocode 2: Design of concrete structures - Part 1-2: General rules - Structural fire design*, Brussels, Belgium., 2004.
[13] F. Bozzoli, A. Mocerino, S. Rainieri, and P. Vocale, 'Inverse heat transfer modeling applied to the estimation of the apparent thermal conductivity of an intumescent fire retardant paint', *Exp. Therm. Fluid Sci.*, vol. 90, pp. 143–152, Jan. 2018, doi: 10.1016/j.expthermflusci.2017.09.006.
[14] R. Yarmohammdian, R. Felicetti, F. Robert, S. Mohaine, and L. Izoret, 'Crack instability of concrete in fire: A new small-scale screening test for spalling', *Cem. Concr. Compos.*, vol. 153, p. 105739, Oct. 2024, doi: 10.1016/j.cemconcomp.2024.105739.
[15] V. Babrauskas, 'The Cone Calorimeter', in *SFPE Handbook of Fire Protection Engineering*, 5th ed., vol. 1, M. J. Hurley, D. Gottuk, J. R. Hall, K. Harada, E. Kuligowski, M. Puchovsky, J. Torero, J. M. Watts, and C. Wieczorek, Eds., New York, NY: Springer New York, 2016. doi: 10.1007/978-1-4939-2565-0.
[16] M. M. Khan, A. Tewarson, and M. Chaos, 'Combustion Characteristics of Materials and Generation of Fire Products', in *SFPE Handbook of Fire Protection Engineering*, M. J. Hurley, D. Gottuk, J. R. Hall, K. Harada, E. Kuligowski, M. Puchovsky, J. Torero, J. M. Watts, and C. Wieczorek, Eds., New York, NY: Springer New York, 2016, pp. 1143–1232. doi: 10.1007/978-1-4939-2565-0_36.
[17] Y. Hasemi, 'Surface Flame Spread', in *SFPE Handbook of Fire Protection Engineering*, M. J. Hurley, D. Gottuk, J. R. Hall, K. Harada, E. Kuligowski, M. Puchovsky, J. Torero, J. M. Watts, and C. Wieczorek, Eds., New York, NY: Springer New York, 2016, pp. 705–723. doi: 10.1007/978-1-4939-2565-0_23.
[18] M. Janssens, 'Calorimetry', in *SFPE Handbook of Fire Protection Engineering*, M. J. Hurley, D. Gottuk, J. R. Hall, K. Harada, E. Kuligowski, M. Puchovsky, J. Torero, J. M. Watts, and C. Wieczorek, Eds., New York, NY: Springer New York, 2016, pp. 905–951. doi: 10.1007/978-1-4939-2565-0_27.
[19] A. Seweryn, A. Lucherini, and J.-M. Franssen, 'An Experimental Apparatus for Bench-Scale Fire Testing Using Electrical Heating Pads', *Fire Technol.*, Dec. 2023, doi: 10.1007/s10694-023-01514-4.
[20] H. Cadosch, D. Morrisset, A. Law, G. Terrasi, and L. Bisby, 'The influence of feedback and convection on imposed heating conditions when using gas-fired radiant panels in fire testing', *Fire Saf. J.*, vol. 141, p. 104013, Dec. 2023, doi: 10.1016/j.firesaf.2023.104013.
[21] C. Maluk, L. Bisby, and G. P. Terrasi, 'Effects of polypropylene fibre type and dose on the propensity for heat-induced concrete spalling', *Eng. Struct.*, vol. 141, pp. 584–595, Jun. 2017, doi: 10.1016/j.engstruct.2017.03.058.

[22] O. Richards, I. Rickard, J. Orr, and L. Bisby, 'Response of concrete cast in permeable moulds to severe heating', *Constr. Build. Mater.*, vol. 160, pp. 526–538, Jan. 2018, doi: 10.1016/j.conbuildmat.2017.11.097.
[23] H. Mohammed, F. Sultangaliyeva, M. Wyrzykowski, G. P. Terrasi, and L. Bisby, 'Heat-induced explosive spalling of self-prestressing, self-compacting concrete slabs', *Constr. Build. Mater.*, vol. 372, p. 130821, Apr. 2023, doi: 10.1016/j.conbuildmat.2023.130821.
[24] A. Elliott, A. Temple, C. Maluk, and L. Bisby, 'Novel Testing to Study the Performance of Intumescent Coatings under Non-Standard Heating Regimes', *Fire Saf. Sci.*, vol. 11, pp. 652–665, 2014, doi: 10.3801/IAFSS.FSS.11-652.
[25] A. Lucherini and C. Maluk, 'Assessing the onset of swelling for thin intumescent coatings under a range of heating conditions', *Fire Saf. J.*, vol. 106, pp. 1–12, Jun. 2019, doi: 10.1016/j.firesaf.2019.03.014.
[26] A. Lucherini, H. Y. Lam, M. Jimenez, F. Samyn, S. Bourbigot, and C. Maluk, 'Fire Testing of Intumescent Coatings: Comparison Between Bench-Scale Furnace and Radiant Panels Experimental Methodologies', *Fire Technol.*, vol. 58, no. 3, pp. 1737–1766, May 2022, doi: 10.1007/s10694-022-01216-3.
[27] A. Lucherini, J. P. Hidalgo, J. L. Torero, and C. Maluk, 'Influence of heating conditions and initial thickness on the effectiveness of thin intumescent coatings', *Fire Saf. J.*, vol. 120, p. 103078, Mar. 2021, doi: 10.1016/j.firesaf.2020.103078.
[28] A. Lucherini, Q. S. Razzaque, and C. Maluk, 'Exploring the fire behaviour of thin intumescent coatings used on timber', *Fire Saf. J.*, vol. 109, p. 102887, Oct. 2019, doi: 10.1016/j.firesaf.2019.102887.
[29] A. Lucherini, J. L. Torero, and C. Maluk, 'Effects of substrate thermal conditions on the swelling of thin intumescent coatings', *Fire Mater.*, vol. 45, no. 7, pp. 952–965, Nov. 2021, doi: 10.1002/fam.2840.
[30] I. Rickard, M. Spearpoint, and S. Lay, 'The performance of laminated glass subjected to constant heat fluxes related to building fires', *Fire Mater.*, vol. 45, no. 2, pp. 283–295, Mar. 2021, doi: 10.1002/fam.2939.
[31] F. Wiesner, F. Randmael, W. Wan, L. Bisby, and R. M. Hadden, 'Structural response of cross-laminated timber compression elements exposed to fire', *Fire Saf. J.*, vol. 91, pp. 56–67, Jul. 2017, doi: 10.1016/j.firesaf.2017.05.010.
[32] J. P. Hidalgo, S. Welch, and J. L. Torero, 'Performance criteria for the fire safe use of thermal insulation in buildings', *Constr. Build. Mater.*, vol. 100, pp. 285–297, Dec. 2015, doi: 10.1016/j.conbuildmat.2015.10.014.
[33] A. Cicione, J. Kruger, R. S. Walls, and G. Van Zijl, 'An experimental study of the behavior of 3D printed concrete at elevated temperatures', *Fire Saf. J.*, vol. 120, p. 103075, Mar. 2021, doi: 10.1016/j.firesaf.2020.103075.
[34] A. D. Botha, R. S. Walls, N. Flores-Quiroz, and A. J. Babafemi, 'Behaviour of concrete building units incorporating waste plastic eco-aggregate (RESIN8) subjected to fire conditions', *J. Build. Eng.*, vol. 76, p. 107393, Oct. 2023, doi: 10.1016/j.jobe.2023.107393.
[35] Y. A. Cengel, 'Radiation Heat Transfer', in *Heat Transfer: A Practical Approach*, 2nd ed., New York: Mcgraw-Hill, 2002, pp. 605–666.
[36] Hukseflux Thermal Sensors, 'User manual SBG01 - Water cooled heat flux sensor'. 2023.
[37] Y. A. Cengel, 'Transient heat conduction', in *Heat Transfer - A Practical Approach*, 2nd ed., New York: Mcgraw-Hill, 2002, pp. 209–264.
[38] T. Gernay *et al.*, 'Experimental investigation of structural failure during the cooling phase of a fire: Concrete columns', *Fire Saf. J.*, vol. 134, p. 103691, Dec. 2022, doi: 10.1016/j.firesaf.2022.103691.

718 [39] CEN, *EN 1991-1-2: Eurocode 1: Actions on structures - Part 1-2: General actions: Actions on*
719 *structures exposed to fire*, Brussels, Belgium., 2002.
720 [40] B. Jovanović *et al.*, 'Experimental investigation on the effect of natural fire exposure on the
721 post-fire behavior of reinforced concrete beams using electric radiant panel', *Struct. Concr.*, p.
722 suco.202400550, Nov. 2024, doi: 10.1002/suco.202400550.
723 [41] J. M. Franssen and T. Gernay, 'Modeling structures in fire with SAFIR®: Theoretical
724 background and capabilities', *J. Struct. Fire Eng.*, vol. 8, no. 3, pp. 300–323, 2017.
725